Ping-pong ball avalanche experiments

J. McElwaine* K. Nishimura

*jim@orange.lowtem.hokudai.ac.jp

Institute of Low Temperature Science,
University of Hokkaido,
North 19 West 8, Kita-Ku,
Sapporo 0060-0819, Japan

In W. D. McCaffrey, B. C. Kneller and J. Peakall, editors
Particulate Gravity Currents, pages 135–148, Blackwell Science (2001)

ABSTRACT

Ping-pong ball avalanche experiments have been carried out for the last three years at the Miyanomori ski jump in Sapporo, Japan, to study three-dimensional granular flows. Up to 550,000 balls were released near the top of the landing slope. The balls then flowed past video cameras positioned close to the flow, which measured individual ball velocities in three dimensions, and air pressure tubes at different heights. The flows developed a complicated three-dimensional structure with a distinct head and tail, lobes and "eyes". "Eyes" have been observed in laboratory granular flow experiments and the other features are similar not only to snow avalanches, but also to other large-scale geophysical flows. The velocities attained showed a remarkable increase with the number of released balls. A power law for this relation is derived by similarity arguments. The air pressure data is used to deduce the structure of the air flow around the avalanche and in conjunction with the kinetic theory of granular matter to estimate the balance of forces in the avalanche head.

Keywords:

snow avalanche, two-phase flow, granular flow

INTRODUCTION

Snow avalanches have been measured and observed in the Shiai valley, Kurobe since 1989. Though there are partial data on the internal velocity distribution for both dense and powder parts (Gubler, 1987; Kawada *et al.*, 1989; Nishimura *et al.*, 1989; Nishimura *et al.*, 1993a; Dent *et al.*, 1994; Nishimura & Ito, 1997) the data are insufficient to constrain and discriminate between current avalanche models, for a recent survey of current models see (Harbitz, 1999, Harbitz (1999)), and thus insufficient to allow a quantitative understanding of the dynamics and internal structure of snow avalanches. The poor quality of the data is because of the unpredictability, scarcity and intense destructive power of avalanches.

Avalanches can be modelled in the laboratory using granular materials on inclined planes, usually in water for powder avalanches (Tochon-Danguy & Hopfinger, 1975; Hopfinger & Tochon-Danguy, 1977; Beghin & Brugnot, 1983; Hermann *et al.*, 1987; Beghin & Olagne, 1991; Keller, 1995) or air for dense avalanches (Hutter, 1991; Hutter *et al.*, 1995; Nishimura *et al.*, 1993b; Greve & Hutter, 1993; Greve *et al.*, 1994). Laboratory experiments are much easier to perform than field experiments and are usually, easily repeatable. However, the small size of the granular particles used makes direct observation of individual particles difficult, and only a few similarity parameters are typically satisfied (Keller, 1995). For example, no laboratory experiments have yet been carried

out in which a dense granular flow becomes a turbulent suspension by entraining the ambient fluid, though in some experiments (Rzadkiewicz *et al.*, 1997) a small number of the grains may enter suspension. Instead experimental models of powder snow models in water tanks use a denser fluid or a premixed turbulent suspension. Laboratory granular flows also rarely exhibit the complex three-dimensional structure which is characteristic of avalanches and other large geophysical flows. For these reasons for the last five years large scale granular flow experiments have been carried out using golf balls and ping-pong balls. The first experiments were carried out on long (20–30 m) chutes and more recently on the Miyanomori ski jump. Ping-pong balls are particularly suitable, since they reach terminal velocity in only a few metres, so fully developed flows occur even on short slopes. These experiments have been described in several papers (Nishimura *et al.*, 1996; Nishimura *et al.*, 1998; Keller *et al.*, 1998).

The aim of these experiments is to elucidate the dynamics of two-phase granular flows rather than to directly extrapolate the results to snow avalanches. The experiments provide detailed data and provide insights on the physically significant dynamical processes controlling avalanches. The hope is that this will lead to a theory of snow avalanches based on physical processes with no free parameters.

The kinetic theory of granular matter provides only poor agreement with experiments (Jenkins & Savage, 1983; Haff, 1983; Lun *et al.*, 1984; Jenkins & Richman, 1988; Johnson *et al.*, 1990; Anderson & Jackson, 1992; Jenkins, 1994), but does provide a theoretical framework for discussing stresses in granular flows. Another approach is the direct simulation of granular flows using the discrete element method (Campbell & Brennen, 1985; Campbell & Gong, 1986; Cleary & Campbell, 1993; Campbell *et al.*, 1995; Hanes *et al.*, 1997). These simulations have increased the understanding of granular flows, including two-phase flows, but these simulations have not yet accurately dealt with particles strongly coupled to fluids or three-dimensional anisotropic flows.

The ping-pong ball avalanches can be described by well known equations. The air flow obeys the Navier-Stokes equations and individual ping-pong balls follow Newton's laws, whereby the force on a particle is a function of gravity, particle-particle contacts, particle-ground contacts and air drag. The no-slip boundary condition between particles and the air flow determine the drag force. For small numbers of particles at low Reynolds numbers in closed domains these equations can be directly solved (Glowinski *et al.*, 1996; Hu, 1996; Blackmore *et al.*, 1999), but for this experiment it is currently impossible, because of the large number of particles and the large range of length and time scales. Particle-particle collisions occur over time intervals of order of 10^{-3} s whereas the duration of the flow in these experiments is around 30 s. The length scales in these experiments are given by the length of the ski jump (160 m), the volume of the flow ($\sqrt[3]{1\,\mathrm{m}^3} = 1\,\mathrm{m}$), the diameter of the balls (0.038 m) and the compression of the balls during collisions (10^{-3} m).

This papers discusses two complementary approaches for describing the experiments. The first is to consider the flow as a single object moving down the ski jump and to use similarity arguments to deduce gross features of the flow. The second approach is to use two-phase flow equations that couple the Navier-Stokes equation for the air flow to the kinetic theory equations for the ball flow using an (empirical) drag force.

EXPERIMENT

The experiments were undertaken at the Miyanomori ski jump (the normal hill for the 1972 Olympics) in Sapporo, Japan. The landing slope was 160 m long and 60 m high (Fig. 1) and covered with an artificial surface. Standard ping-pong balls with a diameter of 38 mm and mass of 2.48 g per ball, were placed in a large box, 15 m or 30 m along from the top of the landing slope. Flow was initiated by opening the hinged door on the front of the box. The balls then flowed down the slope and past the measurement sensors, which were all placed near the middle of the slope 100 m down from the top (83 m from the front of the box). The experimental procedure is described in more detail in (Nishimura *et al.*, 1996).

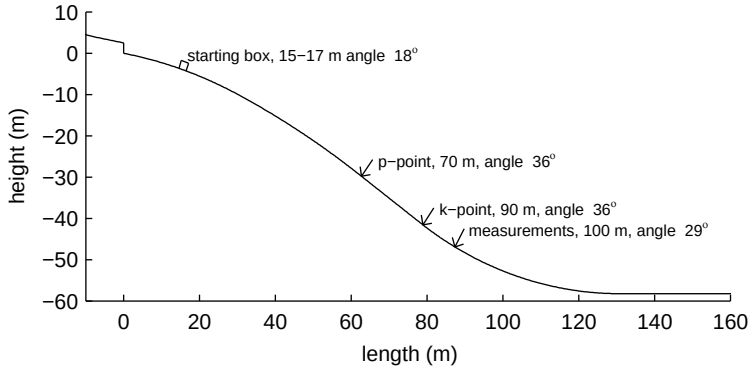

Figure 1: Cross section of the landing slope of the Miyanomori ski jump. Marked distances are measured from the top of the landing slope.

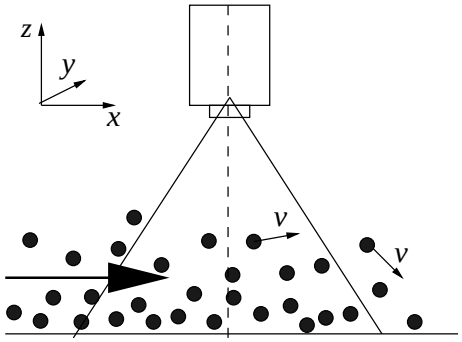

Figure 2: Schematic of the video camera for measuring ball positions

Ball measurements

A video camera was set pointing perpendicularly down at the slope (Fig. 2) at a height of 0.82 m. Balls closer to the lens of the camera appear larger than those which are further away. Thus the z co-ordinate of a ball can be calculated by measuring the size of a ball in the video picture, since all the balls have the same diameter. The x and y co-ordinates of a ball are given directly by its position in the video frame. Comparing positions for the same ball from adjacent video fields gives the three-dimensional velocity of a ball (time-averaged over the 1/60 s between video fields.) The necessary camera corrections and detailed method are described in (Keller *et al.*, 1998).

Air measurements

Measuring air velocity in particulate flows is very difficult. In snow avalanches ordinary meteorological anemometers are inaccurate because of the snow particles, and are usually destroyed (Kawada *et al.*, 1989; Nishimura *et al.*, 1989). (Nishimura *et al.*, 1996) and (Nishimura & Ito, 1997, Nishimura and Ito, (1997)) have developed the use of pressure measurements (sampling frequency 1 KHz) for inferring air speed. A tube connected to a pressure difference sensor is set so that the open end points downwards, perpendicular to the main flow direction. Note that this is not a Pitot tube since each tube has only one opening and the pressure difference is measured with respect to the air pressure some distance from the flow. Bernoulli's law then gives

$$\Delta p = -1/2 \rho_a v^2, \tag{1}$$

where Δp is the pressure difference, ρ_a is the air density and v is the air speed parallel to the slope. However, this equation is only valid when the air flow is perpendicular to the end of the pipe and

the local static pressure is known. Also the sensor itself disturbs the flow. The Reynolds number for the flow around the tube is approximately 10,000 (wind speed 10 m/s, tube diameter 0.01 m), so the flow will be partially turbulent around the sensor. The interaction of the pressure sensor with the flow coupled with the rapid pressure fluctuations as a result of the turbulent flow field would lead to inaccurate measurements, if solely based on Eq. 1. Therefore the pressure tubes were calibrated by measuring the static pressure depression in a wind tunnel over a range of velocities. Four of these air pressure sensors were placed 100 m down the slope at heights of 0.01 m, 0.15 m, 0.3 m and 0.45 m.

Front position

Several video cameras were placed to the side of the slope and at the bottom of the slope. As can be seen in Fig. 3 the leading edge of the avalanche is clearly visible. The position of the front was measured and used to calculate the front velocity.

RESULTS

When the door of the box was opened, the balls at the front of the box rapidly accelerated down the slope (Figs. 3 and 4). The front velocity was much larger than the tail velocity (the last balls took several seconds to leave the box). For a 550,000 ball flow the front of the flow accelerated approximately linearly with distance until it reached a speed of 18 m/s after 65 m, whereas the balls in the tail had a speed of only a few metres per second — similar to the speed of a single ball. The front velocity was roughly constant for the next 30 m until the slope angle started to decrease. This large disparity in speed between head and tail caused the flow to elongate so much that at times it covered more than half the slope. The flows can be separated into three distinct regions: a short, high, fast moving head; a longer, lower body moving at the same speed; and a very long tail moving much slower, consisting of separated balls.

Other macroscopic features of the flow are interesting but hard to quantify. At the beginning of the flow there are often several waves within the flow which move faster than the body and coalesce in the head (Nishimura *et al.*, 1998). Another obvious feature are two roughly circular regions of reduced flow height, symmetrically located about the flow centreline, a little behind the head, called "eyes" after (Nohguchi *et al.*, 1997). They can be seen on the third line up from the bottom of Fig. 3 as the darker regions. Similar patterns have been reported in laboratory granular flow experiments with styrene foam particles (Nohguchi, 1996) and with ice particles (Nohguchi, personal communication). In these experiments the particles are around 1 mm in diameter and the flows contain 1,000–100,000 particles. For such a feature to exist in experiments of such different scales suggests that the mean velocity fields and flow structure are similar in all these experiments. The "eyes" may represent a pair of vortices shed by the head, but only a detailed quantitative analysis of ball velocities can confirm this. In the tail the balls are not distributed evenly but tend to cluster, because of inelastic collapse. (As density in a granular flow increases the collision rate increases thus increasing dissipation and reducing granular pressure. The density thus continues to increase and the collision rate diverges, so that a group of particles can come to rest in continuous contact in finite time.)

Front velocity

In (Nohguchi, 1996, Nohguchi (1996)) granular flows experiments with styrene particles were performed and the front velocity was observed to increase with the number of balls. Similar increases were observed in these experiments. (Nohguchi, 1996, Nohguchi (1996)) deduced that the maximum front velocities, u, for flows which vary only in the number of balls, N, should scale according to

$$u \propto N^{1/6}. \tag{2}$$

In order to derive Eq. 2 the drag force was assumed to be a linear function of the flow velocity. However, the result can be obtained without this assumption as follows.

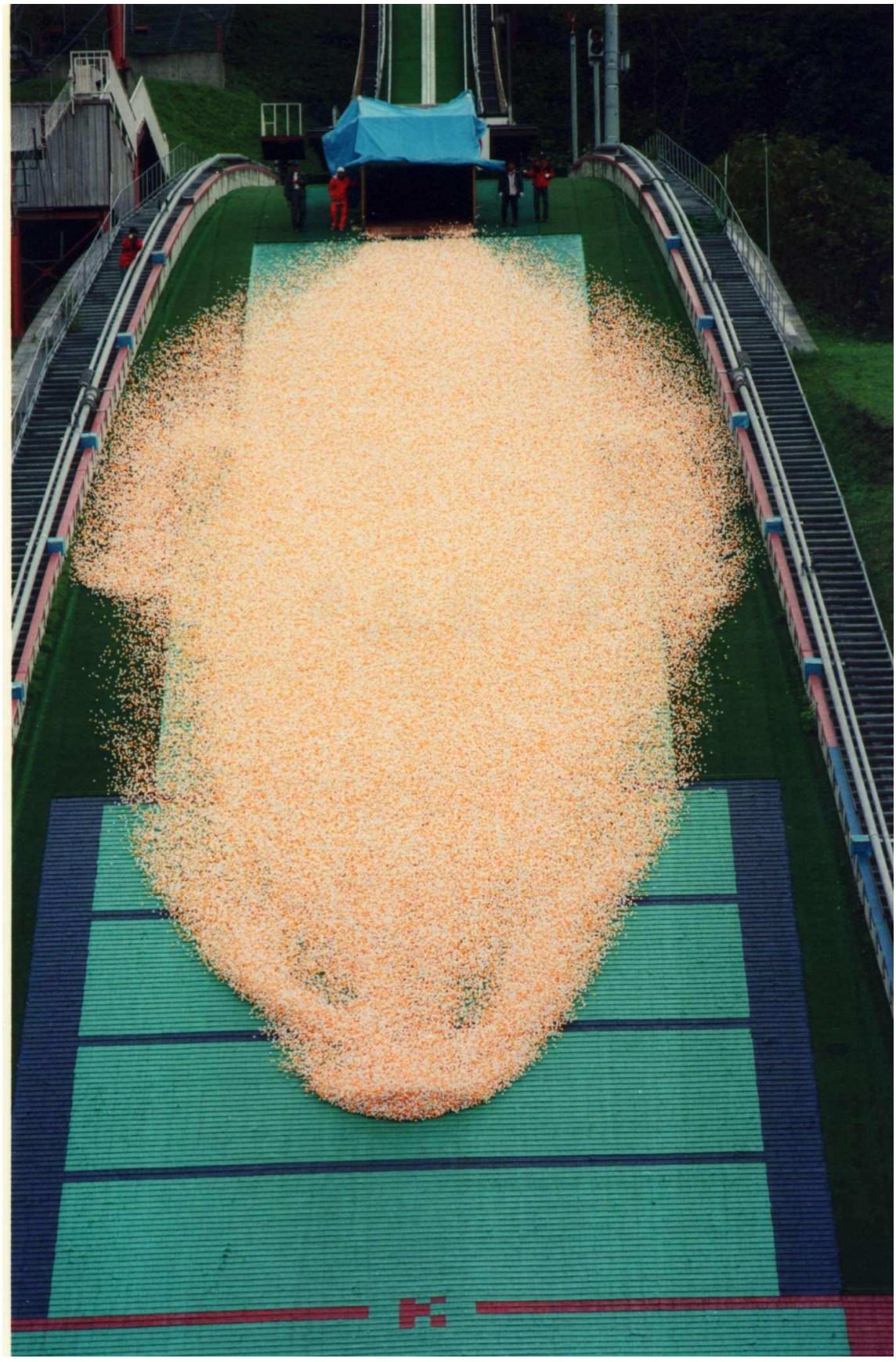

Figure 3: Front view of a 550,000 ball avalanche at the Miyanomori ski jump. The horizontal lines are 5 m apart and the lowest one is 90 m from the top of the landing slope.

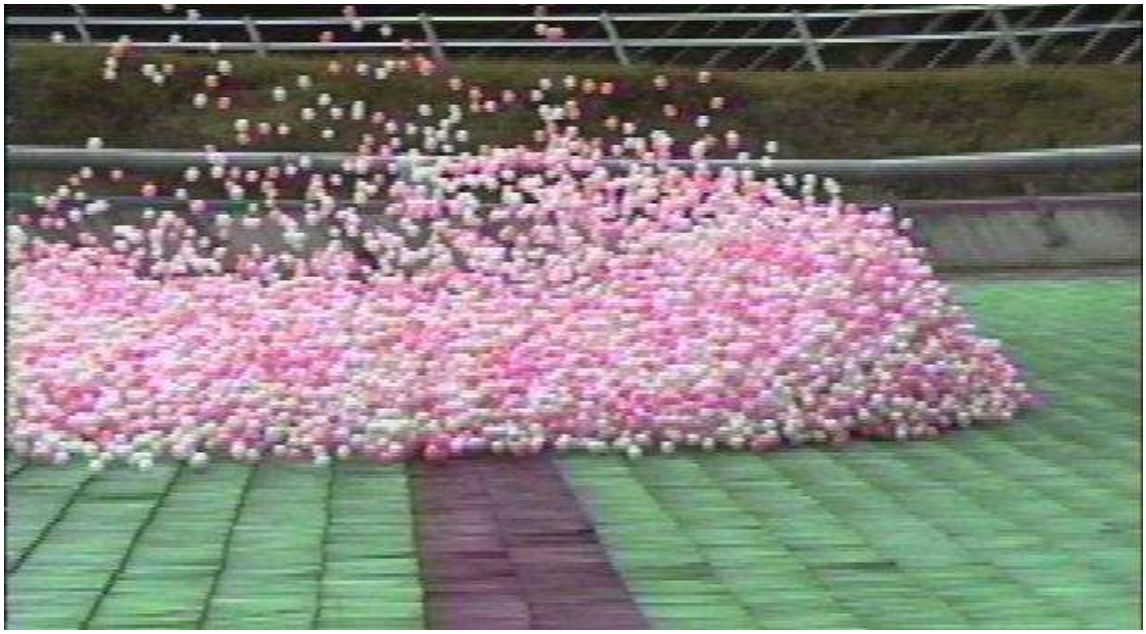

Figure 4: Side view of the head of a 550,0000 ball avalanche at the Miyanomori ski jump.

The critical assumption is that there is only one significant length scale given by

$$L(x) \propto V^{1/3} \propto dN^{1/3}, \tag{3}$$

where V is the volume of all the balls and d the ball diameter. The implied constant of proportionality in Eq. 3 is constant between experiments with different numbers of balls, but is not constant along the slope, i.e. the height and width of the flow at any given position (x) scales with the number of balls. Equation 3 will not be true initially when the input box size is important nor will it be true where the flow is only a few balls thick. However, all the flows with more than $\approx 10,000$ balls are observed rapidly to reach a self-similar shape in around 10 m and the flows are many particle diameters thick except in the tail.

The effective gravitational acceleration on the flow is $g^* = g(1 - \rho_a/\rho_b)(\sin\theta - \mu\cos\theta)$, where θ is the angle of the slope, μ the friction with the slope, g the acceleration due to gravity and ρ_a and ρ_b are the air and ball densities respectively. After the initial surge from the box the flow is close to its equilibrium velocity, i.e. it is accelerating/decelerating slowly, so inertia can be ignored. The Reynolds number for the air flow is of the order 10^6 so air viscosity can be ignored. Under the length scale assumption (Eq. 3) the non-dimensional density ratio $\rho_a V/(Nm)$, where m is the mass of a single ball, is constant for different sized flows since $V \propto N$. Therefore air density ρ_a need not be further considered as a dimensional variable since it can be substituted by m/L^3. The dependence on the box size and ball diameter has already been discussed which leaves only three variables g^*, L and u. Thus the only dimensionless combination that can be formed containing the front velocity is the densiometric Froude number

$$\mathrm{Fr}(x) = \frac{u^2(x)}{L(x)g^*(x)}. \tag{4}$$

This must be constant for different flows thus

$$u(x) = \sqrt{L(x)g^*(x)\mathrm{Fr}(x)} \propto N^{1/6}, \tag{5}$$

since $L \propto N^{1/3}$.

In (Nishimura *et al.*, 1998) the front velocity was measured between the k point and the p point (where the slope angle, 36^o, is roughly constant and steepest, see Fig. 1). The remarkably good

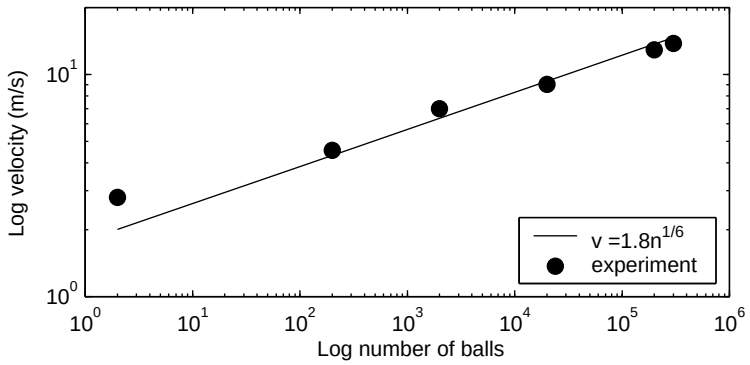

Figure 5: Front velocities at the k-point for different sized avalanches.

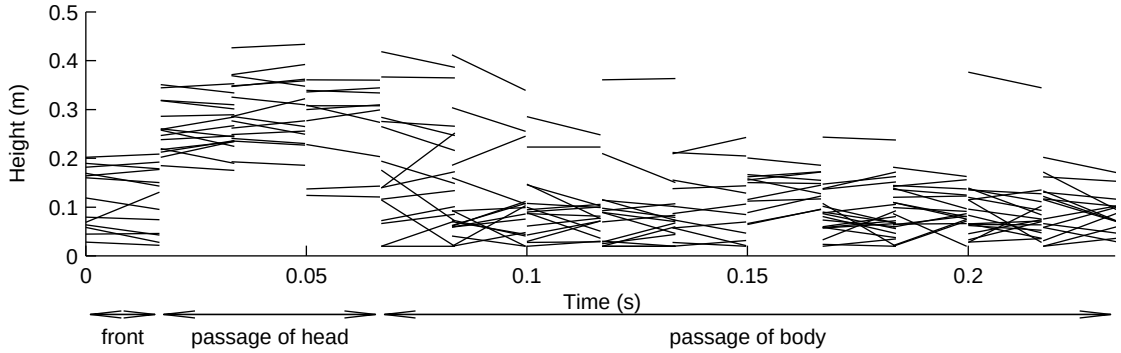

Figure 6: Ball heights in a 200,000 ball avalanche calculated as the balls are advected beneath a fixed video camera. The lines show the ball trajectories from one field to the next.

fit between this equation and experiment is seen in Fig. 5 and provides additional justification for Eq. 3. As expected the error is worse for small flows, since they rapidly spread into single thickness layers with two significant length scales $dn^{1/2}$ (width and length) and d (height). The height is likely to be the significant length scale in this range so for small flows we expect the velocities to be independent of flow size.

Flow structure and ball velocities

By analysing the video film, (Keller *et al.*, 1998) individual particle positions can be calculated, and by identifying balls between adjacent video frames, particle velocities are obtained. Figure 6 shows the perpendicular positions and velocities for a 200,000 ball flow as the particles are advected beneath the camera. The time interval of one profile is 17 ms (1/60 s). This technique, however, cannot see through ping-pong balls, and in the dense head (volume fraction ≈ 0.2) only the balls from the top 0.2 m can be identified thus there is a blank region, marked *passage of the head*, in Fig. 6 where there is no data.

If the structure of any feature in the flow of size l is changing slowly with respect to $l/\overline{u}$, where $\overline{u}$ is the mean flow velocity, then we can regard this data as providing a cross section through the flow in the direction of mean velocity, in this case down the slope. For Fig. 6 the mean flow velocity is 15 m/s thus 0.1 s corresponds to 1.5 m. The head of 1 m long, 0.4 m high followed by a body 0.2 m high is visible. The full flow (not shown in Fig. 6) has a body of approximately constant height 0.2 m and length 10 m followed by the tail of the flow which stretches back to the box and consists of separated balls.

The shape of the velocity profile in a steady shear flow is governed by the relative magnitude of the drag forces on the upper and lower surfaces, the body forces and the vertical transport

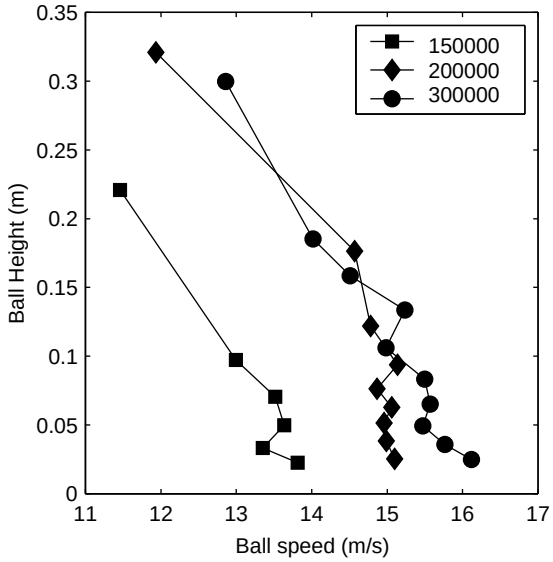

Figure 7: Vertical profile of ball downslope (x) velocity. The height and velocity of each data-point are an average over 50 balls calculated from video camera measurements of the front and body.

rate of momentum. Figure 7 shows that the mean down-slope (x) velocity of the balls decreases monotonically with height. There is no visible velocity reduction at the base indicating that surface friction is unimportant. The mean velocity slowly decreases in the dense part of the flow by around 1 m/s and then very rapidly in the less dense top layer by a further 1–2 m/s. This diffuse, top layer of *saltating* balls moving along approximately parabolic trajectories is visible in Fig. 4 and Fig. 6 and has been discussed in the literature (Johnson *et al.*, 1990). This behaviour is characteristic of *dilute* energetic flows. In high density flows, on the other hand, the top surface is well defined to within a particle diameter. The lower mean velocities of these *saltating* balls is easily explained by the extra air-drag they experience since they move in regions of higher relative air velocity. The relative air velocity in the bulk of the flow must be much lower since the flows are in approximate equilibrium and move up to four times faster than the terminal velocity of an individual ball.

The central part of the ski jump is composed of downslope pointing bristles and experiments with individual balls show that it is totally inelastic — the balls bounce to no observable degree — so that horizontal momentum cannot be converted to vertical momentum by collisions with the slope, but only in collisions with other balls. Since vertical motion will rapidly decay through ground collisions, *a priori*, one might have expected a high density flow where the balls are in continuous contact with very small fluctuation velocities. This is indeed what happens initially when the balls slump out of the box. However, this dense flow state is unstable and as the flow accelerates the velocity fluctuations increase and the density decreases.

The kinetic theory of granular matter follows that of gases and describes a system by a particle distribution function f, where $f(\mathbf{c}, \mathbf{x}, t)\, d\mathbf{c}\, d\mathbf{x}$ is the number of particles with velocity $\mathbf{c}$ and range $d\mathbf{c}$ that are centred at $\mathbf{x}$ and range $d\mathbf{x}$ at time t. The number density $n(\mathbf{x}, t)$ is the integral of f over all velocities and the volume fraction $\phi(\mathbf{x}, t) = n(\mathbf{x}, t)\pi d^3/6$. The mean value of any particle property $\psi(\mathbf{c}, \mathbf{x}, t)$ is defined as

$$\langle \psi \rangle = \frac{1}{n(\mathbf{x}, t)} \int f(\mathbf{c}, \mathbf{x}, t) \psi d\mathbf{c}. \tag{6}$$

The mean velocity field $\mathbf{u}(\mathbf{x}, t)$ is thus $\langle \mathbf{c} \rangle$, the fluctuation velocity $\mathbf{C} = \mathbf{c} - \mathbf{u}$ and the second moment of the fluctuation velocity $K(\mathbf{x}, t) = \langle \mathbf{CC} \rangle$. The granular temperature $T(\mathbf{x}, t) \equiv 1/3(K_{xx} + K_{yy} + K_{zz})$ is the isotropic component of K. The stress tensor (sometimes referred to as the pressure tensor (Jenkins & Savage, 1983)) for a granular flow is

$$\sigma = \phi \rho_b K + m\mathbf{\Theta}[\mathbf{C}], \tag{7}$$

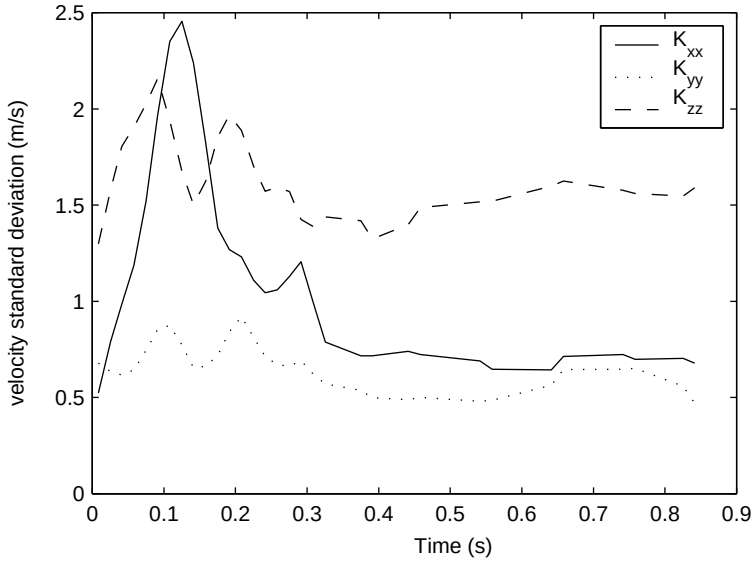

Figure 8: Ball velocity standard deviation for a 300,000 ball experiment. (The data have been smoothed.)

where ρ_b is the ball density, m is particle mass and $\mathbf{\Theta}[\mathbf{C}]$ denotes the collisional transport of velocity fluctuation. The notation follows (Jenkins & Richman, 1988, Jenkins and Richman (1988),) where it is shown that in *dilute* flows the collisional transport term can be ignored. The *dilute* approximation consists of retaining only terms that are constant or linear with respect to volume fraction ϕ and is valid when the strength of mean shear relative to velocity fluctuations is small. This approximation is assumed valid for the rest of the paper.

The square root of the diagonal elements of K are the velocity standard deviations along the coordinate axis and are shown in Fig. 8. The standard deviation is taken over each video field. This shows that the perpendicular (K_{zz}), and cross-slope (K_{yy}) velocity deviations are roughly similar in the head and the body, 1.5 m/s and 0.5 m/s respectively. However, the down-slope (K_{xx}) velocity deviation is low initially, then increases rapidly in the head to reach a maximum of 2.5 m/s before decaying to a roughly constant 0.5 m/s in the body. The results are similar for other flows.

Kinetic theories (Lun *et al.*, 1984; Anderson & Jackson, 1992) of granular matter often postulate that K is isotropic, i.e. the diagonal stresses K_{xx}, K_{yy} and K_{zz} are identical and the off-diagonal stresses are zero. This is clearly not the case for these flows. Figure 8 shows that the diagonal elements of K are never equal. These data are consistent with video footage in which horizontal velocity structure is visible and with Fig. 7 that shows that there is no appreciable vertical shearing.

In the case of steady and uniform flow the mean velocity must be constant and the momentum equation for the flow is

$$\nabla \cdot \phi\rho_b K + \phi\nabla p = \phi\rho_b \mathbf{g} + \phi\mathbf{f} \tag{8}$$

where p is the air pressure, $\mathbf{g}$ is gravity and $\mathbf{f}$ is the drag force from the air on the balls (Jenkins, 1987). For a free surface to be steady and clearly delineated there is a kinematic constraint that $\mathbf{n} \cdot K \cdot \mathbf{n}$ vanishes on the surface, where $\mathbf{n}$ is the surface normal. That is to say as well as the mean velocity vanishing normal to the surface so must the velocity fluctuation. This term, if non-zero, would result in a diffusion outward from the surface of the volume fraction ϕ. The top surface in contrast is diffuse, ϕ slowly decreases with z, and such a condition is not satisfied. Figure 4 shows that the front is indeed very clearly defined which requires that $K_{xx} = 0$. Since K is calculated from averages over two video fields the value at the front is not known, but extrapolating the curve make it plausible that K_{xx} is indeed zero (Fig. 8).

There is also a dynamical requirement given by Eq. 8 that the forces on the front should balance.

$$\frac{\partial \sigma_{xx}}{\partial x} + \frac{\partial \sigma_{xy}}{\partial y} + \frac{\partial \sigma_{xz}}{\partial z} + \phi\frac{\partial p}{\partial x} = \phi f_x - \phi\rho_b g \sin\theta. \tag{9}$$

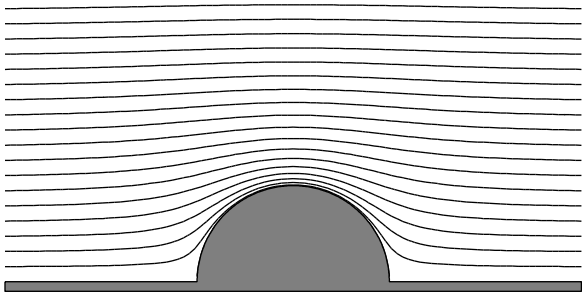

Figure 9: Streamlines for irrotational flow around a stationary sphere.

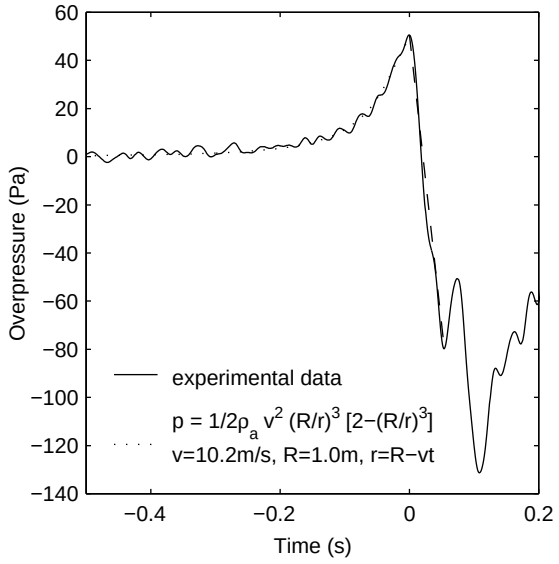

Figure 10: Static air pressure change as the front of a 300,000 ball avalanche is advected past the sensor at height 0.3 m. The balls reached the sensor at $t = 0$ and for $t < 0$ the line of best fit (least mean squares) is drawn assuming the pressure distribution in front of a sphere (two free parameters effective radius R and velocity v).

Unfortunately only a dozen balls or so in each video frame can be identified, which does not provide enough data to calculate y and z derivatives, unless averaged over the whole length of the flow. Assuming that the only z dependence of stress is that required to counteract gravity the $\partial/\partial z$ terms can be dropped. The $\partial/\partial y$ terms should be zero on the centre line ($y = 0$) of the flow and can also also be dropped. The equation is then

$$\frac{\partial \sigma_{xx}}{\partial x} + \phi \frac{\partial p}{\partial x} = \phi f_x - \phi \rho_b g \sin\theta. \tag{10}$$

and can be integrated if f_x is known to provide a variant of Bernoulli's law. This equation will be returned to after a discussion of the air pressure data.

Pressure Measurements

Although in the general case of flow past bodies of arbitrary form the actual flow pattern bears almost no relation to the pattern of potential flow, for *streamlined* shapes the flow may differ very little from potential flow; more precisely, it will be potential flow except in a thin layer of fluid at the surface of the body and in a relatively narrow *wake* behind the body (Landau & Lifschitz,

height (m)	v_1 (m/s)	v_2 (m/s)	$2^{1/6}v_1/v_2$
0.01	7.55	8.16	1.04
0.15	8.21	9.66	0.95
0.30	8.88	10.13	0.98
0.45	6.81	8.96	0.85

Table 1: Comparison of implied velocities for 150,000(v_1) and 300,000(v_2) ball avalanches

height (m)	R_1 (m)	R_2 (m)	$2^{1/3}R_1/R_2$	$2^{\gamma'}R_1/R_2$
0.01	0.76	0.88	1.09	1.02
0.15	0.68	0.80	1.06	1.00
0.30	0.87	1.02	1.08	1.01
0.45	0.98	1.08	1.14	1.07

Table 2: Comparison of implied radii for 150,000(R_1) and 300,000(R_2) ball avalanches

1987). In particular in front of the avalanche head the flow will be irrotational since the Reynolds number is very high (for length of 1 m, velocity 10 m/s, Re $\approx 10^6$). A simple approximation is to assume that the flow field is that of irrotational flow around a sphere (Fig. 9) where the sphere represents the head of the gravity current (cf. Fig. 6) in a stationary frame. The flow field has the required symmetries since it is symmetric about the cross-stream ($y = 0$) plane and, if the influence of the ground on the air-flow is assumed to be small, the flow field can be reflected in the perpendicular ($z = 0$) plane.

A similar approach to the ambient flow around gravity currents was pioneered by (von Kármán, 1940, von Kármán (1940)). He considered the local flow around where the head meets the ground and used this to deduce the head angle (60°). This is accurate over distances small compared to the head height. Similar ideas were also discussed in (Hampton, 1972, Hampton (1972)), but he considered the ambient flow around semi-infinite debris flows, thus his approach is correct over scales large compared to the head height but small compared to the flow length. In contrast the approach in this paper is equivalent to retaining the first three terms (up to the dipole) in a multi-pole expansion and is therefore asymptotically correct.

To apply Bernoulli's theorem it is most convenient to work in a frame in which the flow field can be approximated as steady. This is true in a frame moving with the same velocity as the avalanche head since the slope angle changes slowly. The velocity distribution around a stationary sphere of radius R in a flow field moving with constant velocity $\mathbf{v}$ at infinity is

$$\mathbf{v}(\mathbf{x}) = -\mathbf{v} + \frac{R^3}{2x^3}\left(\frac{3\mathbf{x}(\mathbf{x}\cdot\mathbf{v})}{x^2} - \mathbf{v}\right) \tag{11}$$

Using Bernoulli's theorem the corresponding pressure distribution is

$$\Delta p(\mathbf{x}) = 1/2\rho_a v^2 R^3/x^3\left[2 - R^3/x^3 - 3/4\sin^2\theta(4 - R^3/x^3)\right], \tag{12}$$

where $x\cos\theta = \mathbf{x}\cdot\mathbf{v}$. Regarding the pressure sensors as fixed on the centre line, the data is not of sufficiently high quality to warrant a more complicated approach, then $\mathbf{x}(t) = \mathbf{v}(R/v - t)$, where $t = 0$ is taken as the time when the front reaches the sensor. The output from a pressure sensor is then

$$\Delta p(t) = 1/2\rho_a v^2(1 - vt/R)^{-3}[2 - (1 - vt/R)^{-3}]. \tag{13}$$

Figure 10 shows the result of fitting this curve to the data from one of the sensors. The equation has three free parameters: the impact time, which is taken as the point of highest pressure, the effective radius R, and the effective velocity v. The pressure data was sampled at 1000 Hz and passed through a 4 ms width Gaussian filter, ρ_a was taken as 1.2 Kg/m^3 and an additional correction was applied after calibrating the sensors in the wind tunnel.

The velocities implied by the pressure data are shown in table 1. The lower three sensors are all in rough agreement with the velocity increasing slightly with height. The difference between

these velocities and the video derived head velocity (of order 5 m/s) is the penetration velocity of the air into the head. Unsurprisingly this decreases with height as the air flows over the avalanche rather than into it. The flow velocities from the top sensor (height 0.45m) are low because it is largely out of the flow in a region of reduced air velocity. The third column of table 1 compares the air velocities with scaling Eq. 2. The agreement for the lowest three sensors in the flow is very good and provides further evidence in favour of the length scaling hypothesis.

Though the calculated velocities match the scaling law reasonably well the radii do not (Table 2). A possible explanation is as follows. The flow field far from the body is that of a dipole imposed on constant flow. The magnitude of the dipole is the surface area of the implied sphere times the velocity $\pi R^2 u$. Close to the front however the flow field, to second order, will be more like that around an ellipsoid (this is the result of expanding the surface to second order in the coordinates). The equation fit is influenced by the region of high pressure difference close to the flow front and the length scale measured here is actually the local radius of curvature. Thus $1/R = 1/R_1 + 1/R_2$. Video footage and pictures of the slope shows that the flow front is reasonably approximated by the parabola $y = x^2/d$ where $d = 5\,\mathrm{m}$ and y is the distance from the centre line. Thus in Fig. 3 it can be seen that 5 m back from the front the flow is 10 m wide. The measure radius of curvature in the x-y plane is thus $R_2 = d/2 = 2.5\,\mathrm{m}$ *independent of the flow scale.* This does not necessarily contradict the scaling hypothesis, because this is a local length scale and the width of the flow is still expected to scale as $N^{1/3}$. Thus if R_1 scales and R_2 is constant the ratio between front radii is

$$\begin{aligned} R'/R &= \frac{1/R_1 + 1/R_2}{1/(\lambda R_1) + 1/R_2} \\ &= \lambda \left[1 + \frac{\lambda - 1}{1 + R_2/R_1}\right]^{-1} \end{aligned}$$

where $\lambda = (N'/N)^{1/3}$ the length scaling ratio. When λ is close to 1 this can be simplified to

$$R'/R = \lambda^{R_2/(R_1+R_2)} + O((1-\lambda)^2) \tag{14}$$

thus the scaling exponent $\gamma = 1/3$ is altered to $\gamma' = \gamma/(1 + R_1/R_2)$. To the same order of approximation R_1 can be taken from the flows for either N or N'. The fourth column of table 2 shows the much better fit obtained with this analysis $R_2/R_1 = 2.5$ and $\gamma' = 5/21$. This is a very tentative solution and an explanation is still required as to why the front should have a constant parabolic shape.

The definition of the calculated radius is somewhat arbitrary. The pressure data could be equivalently fitted to

$$\Delta p(t) = 1/2 \rho_a v^2 (1 - t/t_0)^{-3} [2 - (1 - t/t_0)^{-3}] \tag{15}$$

where t_0 is a time constant. The radius is then deduced from $R = t_0 v$. The above analysis took v as the air velocity, but a more natural choice would be to use the velocity of the coordinate frame, that is the front velocity u if this is known. Since this velocity has the same scaling this would only result in the implied radii being multiplied by some constant factor, thus the previous discussion is unaffected.

Air pressure through the front

Within the ping-pong ball flow the steady-state mass and momentum equations for the air flow are

$$\nabla \cdot (1 - \phi)\mathbf{v} = 0, \tag{16}$$

$$\rho_a (1 - \phi)(\mathbf{v} \cdot \nabla)\mathbf{v} + (1 - \phi)\nabla p = -\phi \mathbf{f}. \tag{17}$$

To calculate the pressure inside the flow these equations must be integrated. A simple approximation for the force valid to lowest order in ϕ is

$$\mathbf{f} = \rho_a v^2 / \alpha \tag{18}$$

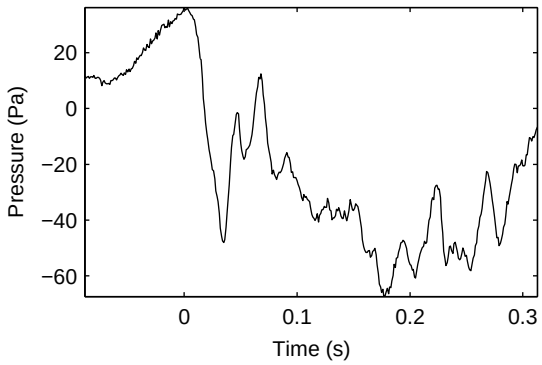

Figure 11: Air pressure through the front at 0.01 m for 300,000 balls. The front reaches the sensor at $t = 0\,\mathrm{s}$.

where $\alpha = \rho_a u_T^2/(\rho_b - \rho_a)g = 0.08\,\mathrm{m}$ an air drag length scale and u_T is the terminal velocity of an individual ball ($7.5\,\mathrm{m/s}$). An analytic solution is not easy to find. However, if the streamlines are not diverging (or converging) too rapidly the continuity equation can be approximated by $(1-\phi)\mathbf{v} = \mathbf{v}_0$ over short distances if the streamlines diverge slowly, where $\mathbf{v}_0$ is the penetration velocity of the air into the front. This is most likely to be true close to the ground where symmetry suggests there will be a streamline passing straight through the centre of the flow. Substituting this into Eq. 17 and integrating along this streamline

$$p = p_0 - v_0^2\rho_a\phi - v_0^2\rho_a/\alpha \int_0^x \phi(s)\mathrm{d}s + O(\phi^2), \tag{19}$$

where s is distance along a streamline. Even if the surface of the flow is sharply defined to within a ball diameter ϕ changes more slowly because it is defined as an average over a volume containing many balls. Suppose the ball concentration is 0 outside the flow and ϕ_c constant inside the flow. Then ϕ increases linearly from 0 to ϕ_c over a width w of order $d\phi_c^{-1/3}$. Then integrating Eq. 19 gives

$$p - p_0 = -v_0^2\phi_c\rho_a \begin{cases} 2\frac{s}{w}\left(1+\frac{s}{2\alpha}\right) & s \le w \\ \left(1+\frac{2s-w}{2\alpha}\right) & s \ge w. \end{cases}, \tag{20}$$

accurate for small s. Over longer distances the streamlines will diverge, as the air flow is deflected up and out of the avalanche, the velocity will decrease and the pressure will increase (see Fig. 11.)

The rapid decrease in pressure as the flow front goes past the sensor that is predicted by this equation is clearly seen in Fig. 11 (and also Fig. 10). The total pressure drops by 84 Pa from 0 s to 0.035 s. The front velocity is around 15 m/s so this corresponds to a distance of 0.5 m certainly much larger than w thus Eq. 20 is $v_0^2\phi_c \approx 9$. From table 1 the air velocity for this flow at 0.01 m is 8 m/s thus $v_0 = 7\,\mathrm{m/s}$ so that $\phi_c \approx 0.2$. This value for the volume fraction seems reasonable and is much lower than the maximum packing fraction thus justifying the dilute approximation.

The x momentum equation for the ping-pong balls (Eq. 8) can now be integrated with the same approximations to give

$$K_{xx}(x) = [p(0) - p(x)]/\rho_b + x\frac{\rho_a v_0^2}{\rho_b \alpha} - xg\sin\theta \tag{21}$$

At $t = 0.035\,\mathrm{s}$ (using linearly interpolation) $K_{xx} = 1.9\,\mathrm{m^2/s^2}$, $(p(0) - p(x))/\rho_b = 0.96\,\mathrm{m^2/s^2}$ and $x\frac{\rho_a v_0^2}{\rho_b \alpha} = 4.5\,\mathrm{m^2/s^2}$ and $xg\sin\theta = 2.5\,\mathrm{m^2/s^2}$. These quantities are of the same order showing that the structure of the head is determined by the balance between air drag, granular stress and gravity. Further back in the body of the avalanche K_{xx} is approximately constant and the pressure varies only slowly. Since the effect of surface drag appears to be small this implies that the air drag on the top surface balances gravity.

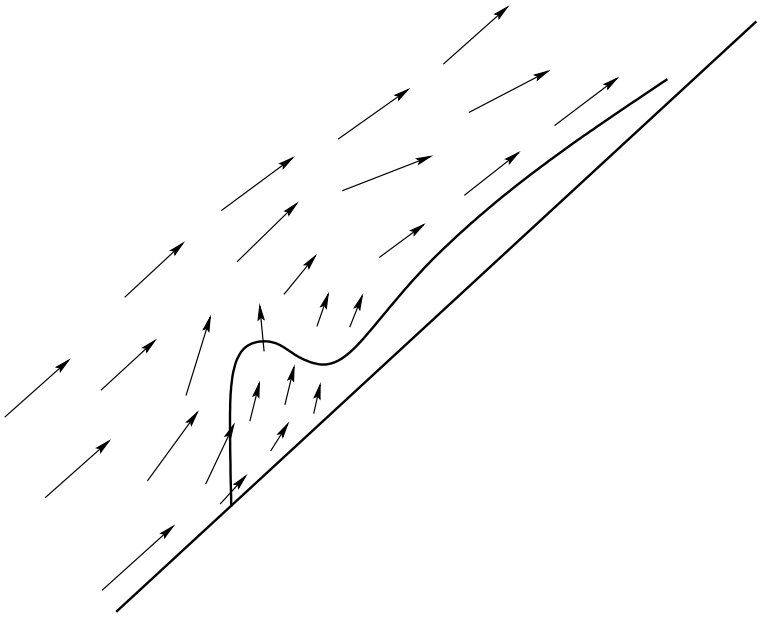

Figure 12: Schematic of the air flow round and through a ping-pong ball avalanche.

A more detailed analysis of Eq. 21 is not appropriate for several reasons. The large fluctuations of the air pressure in the avalanche imply that the flow is turbulent and make interpretation of the air pressure data very difficult since the sensor measures a complicated function of the local velocity and local pressure which can only be simply understood if the direction of the velocity is known. The ball velocity data also contains a lot of noise since in a typical frame only a dozen balls can be identified. Though mean values of velocity are reasonably accurate derivatives of K are much less so. There is an additional problem that the balls that can be identified may be very special (perhaps only those with low vertical velocity have been sampled for example) possibly leading to systematic errors which have not been estimated. In addition the ball position measurements were taken one metre to the left of the flow centre and the location of the pressure measurements. Despite all these difficulties the data does suggest a number of significant processes within the avalanches.

DISCUSSION

Classical work on gravity currents is based on perfect-fluid theory and assumes that the effects of viscosity and mixing of the fluids at the interface can be ignored (Benjamin, 1968). A major result of Benjamin (1968) is that, except when a gravity current exactly fills half a cavity, energy dissipation must occur through the formation of a head and turbulent flow behind it. Extensions to the basic theory include lower boundary effects (Simpson, 1972) and a mixing region behind the head (Simpson, 1986), but there is still assumed to be a clear boundary at the front of the current.

A complete description of the flow field for a mixture of *Newtonian* fluids requires only one velocity field. This is because there can be no relative motion (at a point) between two fluids since a no-slip condition holds everywhere, thus the velocity fields for each fluid (where they are defined) must be identical. Thus mixing between fluids is a slow diffusion process and there are often well defined boundaries. The stability of boundaries is also enhanced by surface tension. However, when one of the fluids is a non-cohesive granular fluid there is no surface tension and the granular fluid will generally have a distinct velocity field. This is because although on the surface of each grain a no slip condition holds, very large velocity gradients can exist across a narrow boundary layer, thus the difference between the ambient fluid velocity field and the granular velocity field averaged over volumes containing a few grains can be very large. For grains falling in a gravitational field

for example the relative velocity will be of the order of the terminal velocity.

The standard gravity current theory (Benjamin, 1968) (correctly) assumes a stagnation point at the front of a gravity current because the velocity of the ambient and the current must be equal. This need not be true for granular gravity currents and the air pressure data shows that there is a significant relative velocity over the width of the head (Fig. 12.) The drag force is related to the relative velocity so a large difference between these avalanches and standard gravity currents is that the drag is a body force over the head of the avalanche rather than a surface force over the head's front surface. Analysis of the forces in the head of the avalanches shows that there is an approximate balance of forces on the balls between gravity, granular stress and air drag, and that surface friction is negligible. The air drag is balanced by a large, anisotropic increase in the granular stress and gravity. This increase is a result of an increase in the downslope fluctuation velocity which then leads to an increase in vertical and cross-slope fluctuations through collisions. Though a quantatitive balance of the vertical forces in the head has not been accomplished the granular stress and the vertical component of the drag are probably both significant and lead to the height of the flow. Air drag may also directly enhance vertical velocity fluctuations. Further back in the body of the avalanche the granular stresses are constant (downslope) and the height is lower. Since surface drag is negligible the gravity must be balanced by air drag forces through the top surface. A likely mechanism for this is momentum transfer by the saltating particles. During their high trajectories they have time to exchange considerable horizontal momentum with slowly moving air and when they collide with the main body this momentum will be almost perfectly transfered. In effect there is a drag interaction between the main body and the air flow over the whole height of the saltating balls. Though this has not been quantified, this mechanism of momentum transfer is most likely more efficient than the drag on the upper surface of a smooth gravity current and helps explains why steady flows occur on such steeps slopes even with such a large relative density ($\rho_b/\rho_a \approx 90$.)

CONCLUSIONS

The air pressure distribution in front of the ping-pong ball avalanches is well approximated by irrotational flow around around a sphere. This approach could be extended to the flow behind the head by comparing the data with turbulent wake theory, but this is difficult because of the complicated interaction of the pressure sensors with the air flow when the velocity direction is unknown. The implied air velocities scale as the sixth power of the number of balls in agreement with dimensional analysis and the scaling for the ping-pong ball velocities. The length scales implied by the air flow are of the same order of magnitude as the front height, but only obey the scaling law if the shape of the head is assumed to have a constant curvature (in the plane of the slope). Kinetic theory calculations show a quantatitive balance of forces in the head between gravity, granular stress and air drag.

ACKNOWLEDGEMENTS

The authors gratefully thank the many people who came to Miyanomori for the experiment, which could not have been done without their help. Furthermore we wish to thank the workshop staff of the Institute of Low Temperature Science who made the equipment. This work was partly supported by grant-in-aid for cooperative research and science from the Japanese Ministry of Education, Science and Culture. One of the authors was supported by an EU/JSPS Fellowship.

NOMENCLATURE

α	Air drag length scale
$\mathbf{c}$	Ball velocity
$\mathbf{C}$	Ball fluctuation velocity
d	Ball diameter
f	Position and velocity distribution function
$\mathbf{f}$	Drag force between balls and air
Fr	Froude number
$\mathbf{g}, g$	Gravity
g^*	Gravity adjusted for buoyancy, friction and slope angle
γ	Scaling exponent
K	Second moment of ball fluctuation velocity
l	Length of a feature in the flow
L	Length scale of a flow
λ	Length scale ratio
m	mass of an individual ball
μ	Ball-slope friction
$\mathbf{n}$	Surface normal
n	Ball number density
N	Number of balls in an experiment
p	Air pressure
p_0	Air pressure at the flow front
ϕ	Ball volume density
ϕ_0	Constant ball volume density in the flow
ψ	General function of balls
r	Distance from centre of flow sphere
R	Radius of sphere
R_1, R_2	Radii of curvature
ρ_a	Air density
ρ_b	Ball density
σ	Stress tensor
s	Distance along a streamline
t	Time
t_0	Time constant
T	Granular temperature
θ	Slope angle
θ_x, θ_y, θ_z	Rotations of the principal axes of K from the coordinate axes
$\mathbf{u}$	Mean ball velocity
u	Speed of the flow front
$\overline{u}$	Mean speed of the flow
$\mathbf{v}, v$	Air velocity and speed
$\mathbf{v}_0$, v_0	Relative velocity and speed between air and flow front
w	Width of the ball volume density variation
$\mathbf{x} = (x, y, z)$	Local Cartesian coordinates aligned with the slope

References

Anderson, K. G. and Jackson, R. (1992) A comparison of the solutions of some proposed equations of motion of granular materials for fully developed flow down inclined planes. *J. Fluid Mech.*, **241**, 145–168.

Beghin, P. and Brugnot, G. (1983) Contributions of theoretical and experimental results to powder-snow avalanche dynamics. *Cold Reg. Sci. Tech.*, **8**, 67–73.

Beghin, P. and Olagne, X. (1991) Experimental and theoretical study of the dynamics of powder snow avalanches. *Cold Reg. Sci. Tech.*, **19**, 317–326.

Benjamin, T. B. (1968) Gravity currents and related phenomena. *J. Fluid Mech.*, **31(2)**, 209–248.

Blackmore, D., Samulyak, R., and Rosato, A. D. (1999) New mathematical models for particle flow dynamics. *Nonlin. Math. Phys.*, **6(2)**, 198–221.

Campbell, C. S. and Brennen, C. E. (1985) Computer simulations of granular shear flows. *J. Fluid Mech.*, **151**, 167–188.

Campbell, C. S., Cleary, P. W., and Hopkins, M. (1995) Large-scale landslide simulations: Global deformation, velocities and basal friction. *J. Geophys. Res.*, **100**, 8267–8283.

Campbell, C. S. and Gong, A. (1986) The stress tensor in a two-dimensional granular shear flow. *J. Fluid Mech.*, **164**, 107–125.

Cleary, P. W. and Campbell, C. S. (1993) Self-lubrication for long runout landslides: Examination by computer simulation. *J. Geophys. Res.*, **98(B12)**, 21911–21924.

Dent, J. D., Adams, E., Bailey, I. J., Jazbutis, T. G., and Schmidt, D. S. (1994) Velocity and mass transport measurements in a snow avalanche. In *International Snow Science Workshop, 30 October – 3 November 1994, Snowbird, Utah*, pages 347–369. Snowbird, UT, P.O. Box 49. American Association of Avalanche Professionals.

Glowinski, R., Pan, T. W., and Periaux, J. (1996) Fictitious domain methods for incompressible viscous flow around moving rigid bodies. In Whiteman, J. R., editor, *The Mathematics of Finite Elements and Applications, Highlight 1996*, pages 155–174. Wiley.

Greve, R. and Hutter, K. (1993) Motion of a granular avalanche in a convex and concave curved chute: Experiments and theoretical predictions. *Phil. Trans. R. Soc. Lond. A*, **342**, 573–600.

Greve, R., Koch, T., and Hutter, K. (1994) Unconfined flow of granular avalanches along a partly curved surface. I. Theory. *Proc. R. Soc. Lond. A*, **445**, 399–413.

Gubler, H. (1987) Measurements and modelling of snow avalanche speeds. In *Avalanche formation, movement and effects (Proceedings of the Davos Symposium September 1986)*, pages 405–420, Wallingford. IAHS.

Haff, P. K. (1983) Grain flow as a fluid-mechanic phenomenon. *J. Fluid Mech.*, **134**, 401–430.

Hampton, M. A. (1972) The role of subaqueous debris flow in generating turbidity currents. *J.Sed.Pet.*, **42(4)**, 775–793.

Hanes, D. M., Walton, O., Zakirov, V., Locurto, G., and Bucklin, R. (1997) Observations and simulations of the flow of nearly-ellipsoidal, inelastic particles down a bumpy incline. In *Proceeding of the Third International Conference on Powders & Grains*, pages 459–461, Rotterdam. A A Balkema.

Harbitz, C. B. (1999) Snow avalanche modelling, mapping and warning in Europe. deliverable no.4: A survey of computational models for snow avalanche motion. Technical Report 581220-1, Norwegian Geotechnical Institute.

Hermann, F., Hermann, J., and Hutter, K. (1987) Laboratory experiments on the dynamics of powder snow avalanches. In *Avalanche formation, movement and effects (Proceedings of the Davos Symposium September 1986)*, pages 431–430, Wallingford. IAHS.

Hopfinger, E. J. and Tochon-Danguy, J.-C. (1977) A model study of powder snow avalanches. *J. Glaciol.*, **19(81)**, 343–356.

Hu, H. H. (1996) Direct simulation of flows of solid-liquid mixtures. *Int. J. Multiphase Flow*, **22(2)**, 335–352.

Hutter, K. (1991) Two- and three-dimensional evolution of granular avalanche flow — theory and experiments revisited. *Acta Mech.*, Suppl **1**, 167–181.

Hutter, K., Koch, T., Plüss, C., and Savage, S. B. (1995) The dynamics of avalanches of granular materials from initiation to runout. part ii: Experiments. *Acta Mech.*, **109**, 127–165.

Jenkins, J. T. (1987) Kinetic theory for nearly elastic spheres. In Herrmann, H. J., Hovi, J.-P., and Luding, S., editors, *Physics of Dry Granular Media*, pages 353–370. Kluwer.

Jenkins, J. T. (1994) Rapid granular flow down inclines. *Appl. Mech. Rev.*, **47(6)**, 240–244.

Jenkins, J. T. and Richman, M. W. (1988) Plane simple shear of smooth inelastic circular disks: the anisotropy of the second moments in the dilute and dense limits. *J. Fluid Mech.*, **192**, 313–328.

Jenkins, J. T. and Savage, S. B. (1983) A theory for the rapid flow of identical, smooth, nearly elastic, spherical particles. *J. Fluid Mech.*, **130**, 187–202.

Johnson, P. C., Nott, P., and Jackson, R. (1990) Frictional-collisional equations of motion for particulate flows and their application to chutes. *J. Fluid Mech.*, **210**, 501–535.

von Kármán, T. (1940) The engineer grapples with nonlinear problems. *Bull. Am. Math. Soc.*, **46**, 615–683.

Kawada, K., Nishimura, K., and Maeno, N. (1989) Experimental studies on a powder-snow avalanche. *Ann. Glaciol.*, **13**, 129–234.

Keller, S. (1995) Measurements of powder snow avalanches - laboratory -. *Surv. Geophys.*, **16(5/6)**, 661–670.

Keller, S., Ito, Y., and Nishimura, K. (1998) Measurements of the velocity distribution in ping-pong ball avalanches. *Ann. Glaciol.*, **26**, 259–264.

Landau, L. D. and Lifschitz, E. M. (1987) *Fluid Mechanics*, volume 6 of *Course of Theoretical Physics*, pp. 16. Butterworth-Heinenann, Oxford, 2nd edition.

Lun, C. K. K., Savage, S. B., Jeffrey, D. J., and Chepurniy, N. (1984) Kinetic theories for granular flow: inelastic particles in couette flow and slightly inelastic particles in a general flow field. *J. Fluid Mech.*, **140**, 223–256.

Nishimura, K. and Ito, Y. (1997) Velocity distribution in snow avalanches. *J. Geophys. Res.*, **102(B12)**, 27297–27303.

Nishimura, K., Narita, H., and Maeno, N. (1989) The internal structure of powder-snow avalanches. *Ann. Glaciol.*, **13**, 207–210.

Nishimura, K., Maeno, N., Kawada, K., and Izumi, K. (1993a) Structures of snow cloud in dry-snow avalanches. *Ann. Glaciol.*, **18**, 173–178.

Nishimura, K., Kosugi, K., and Nakagawa, M. (1993b) Experiments on ice-sphere flows along an inclined chute. *Mech. Mat.*, **16**, 205–209.

Nishimura, K., Nohguchi, Y., Ito, Y., Kosugi, K., and Izumi, K. (1996) Snow avalanche experiments at ski jump. In *International Snow Science Workshop, 6–10 October 1996, Banff, Canada*, pages 244–251, P.O. Box 2759, Revelstoke, B.C. Canadian Avalanche Association.

Nishimura, K., Keller, S., McElwaine, J., and Nohguchi, Y. (1998) Ping-pong ball avalanche at a ski jump. *Granular Matter*, **1(2)**, 51–56.

Nohguchi, Y. (1996) Avalanche experiments with styrene foam particles. In *Proceedings of the Third International Conference on Snow Engineering (ICSE-3),Sendai, Japan*, pages 63–68.

Nohguchi, Y., Ozawa, H., and Nishimura, K. (1997) 3-d experiments of light granular avalanches. In *Proceedings, 1997 Meeting of Japan Society of Fluid Mechanics*, pages 421–422. in Japanese with English abstract.

Rzadkiewicz, S. A., Mariotti, C., and Heinrich, P. (1997) Numerical simulation of submarine landslides and their hydraulic effects. *J. Waterway, Port, Coastal, and Ocean Eng.*, **123(4)**, 149–157.

Simpson, J. E. (1972) Effects of the lower boundary on the head of a gravity current. *J. Fluid Mech.*, **53(4)**, 759–768.

Simpson, J. E. (1986) Mixing at the front of a gravity current. *Acta Mech.*, **63**, 245–253.

Tochon-Danguy, J.-C. and Hopfinger, E. J. (1975) Simulations of the dynamics of powder snow avalanches. In *Proceeding of the Grindelwald Symposium April 1974 — Snow Mechanics*, pages 369–380, Wallingford. IAHS.